Herpetological Journal SUPPLEMENTARY MATERIALS

Published by the British Herpetological Society

Dark future for a black salamander: effects of climate change and conservation implications for an endemic alpine amphibian

Davide Giuliano, Daniele Seglie, Paolo Eusebio Bergò, Riccardo Cavalcante, Marco Favelli, Bruno Aimone Gigio, Alain Bloc, Anna Gaggino, Matteo Massara, Alessandra Pucci, Marco Rastelli, Claude Miaud & Barbara Rizzioli

CONTENTS

APPENDIX S1 – Supplementary methods

1. *Calibration area and study area*

According to Soberón & Peterson (2005), species' geographic distribution mainly depends on three interacting factors: biotic (*B*), abiotic (*A*) and movement (*M*). In this framework, a species is supposed to naturally occur only in those parts of the world that have been accessible via dispersal throughout its biogeographical history (*M*), especially where and when both biotic (*B*) and abiotic (*A*) conditions are suitable for its survival. Therefore, *M* corresponds to the whole area where a species is potentially present, where the effect of the environmental predictors (*B* and *A*) has to be tested when performing species distribution modelling. Indeed, a proper identification of *M* has important implications on model parameterization, model validation and model comparisons, thus justifying the recommendation that *M* should be considered entirely when setting model calibration areas (Barve et al., 2011).

In the case of the Lanza's alpine salamander, the *M* area can be identified hypothesizing four major geographical barriers that might have conditioned the distribution of this amphibian in the Western European Alps (between Italy and France), even confirmed by the species' genetic structure: the Susa Valley (North), the Po Plane (East), the Monviso Massif (South), and the Durance Valley (West). Accordingly, the rectangular area selected to calibrate the models (hereafter "calibration area"; 3433 Km^2) is included between the following geographical limits: 45.12° N (North); 7.4° E (East); 44.56° N (South); 6.7° E (West) (Fig. S1.1). Since occurrence data and targeted field surveys proved that the current distribution of *Salamandra lanzai* actually covers only a portion of the calibration area, a subset area (assumed to correspond to the G_0 area, *sensu* Peterson et al., 2011; hereafter "study area"; 778 Km^2, Fig. S1.2) was identified following an expert-based approach, in order to increase the reliability of the spatial analyses carried out on model outputs (i.e. to ensure a better fit with the actual species distribution). In particular, all the known *S. lanzai*'s populations were included in the study area, drawing borders on the main surrounding mountain ridges (mostly above 2600 m a.s.l.), supposed to represent a dispersal barrier for the species, and following on the other side the 1200 m-contour line, corresponding to the lowest elevation of occurrence reported for this amphibian (Andreone, 2006). In addition, the predicted suitable areas where the Lanza's alpine salamander was not found during the field validation procedure were excluded from the study area, especially those located on the edge of the known distribution range.

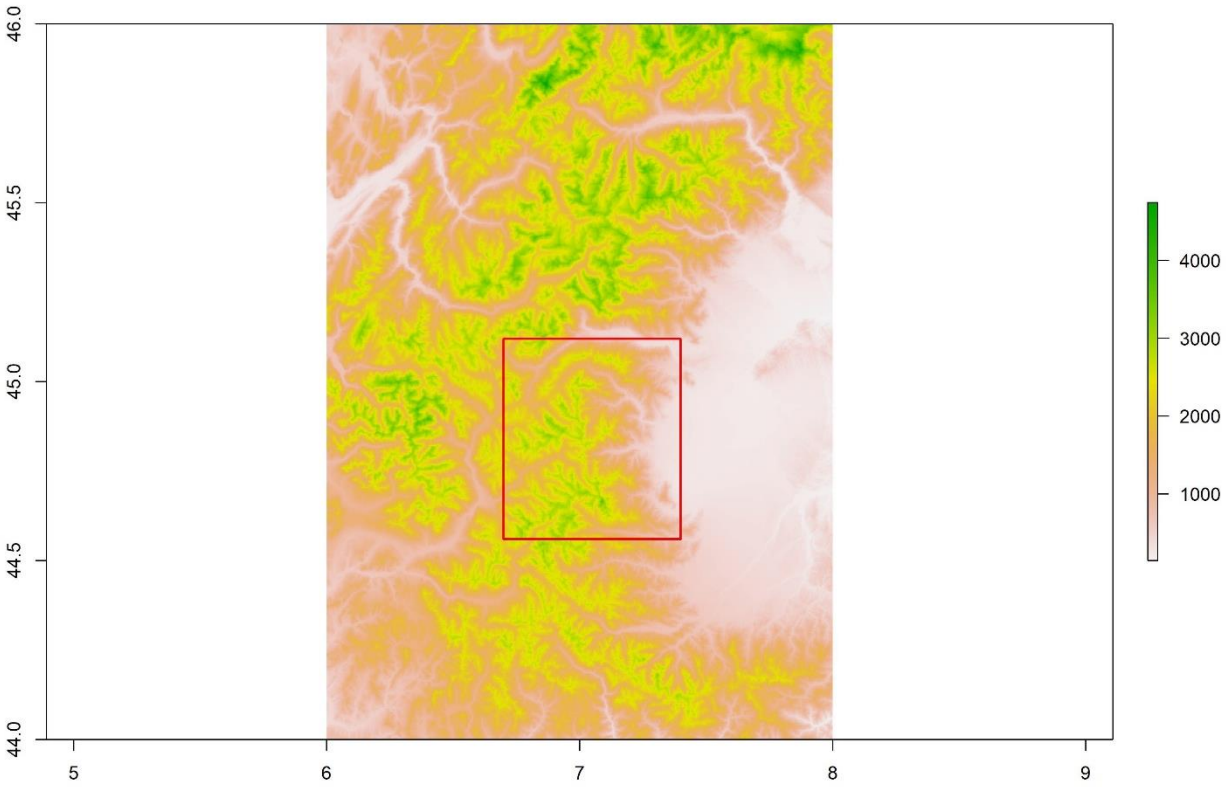

Figure S1.1 Physical map (Digital Terrain Model) representing the Western European Alps. The red square encompasses the model calibration area considered in this study. The x and y axes report longitude and latitude respectively (decimal degrees), while elevation (in metres) is highlighted with different colours (see legend).

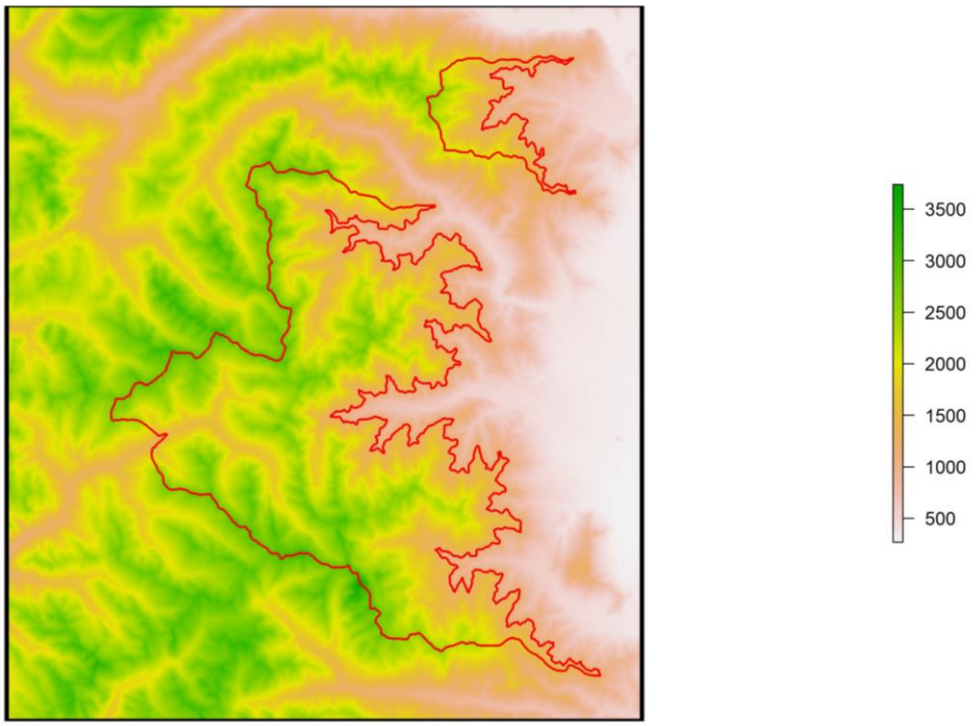

Figure S1.2 Physical map (Digital Terrain Model) representing the calibration area used in the modelling procedure concerning the Lanza's alpine salamander (black box). The red line encompasses the study area used as reference for spatial analyses. Elevation (in metres) is highlighted with different colours (see legend).

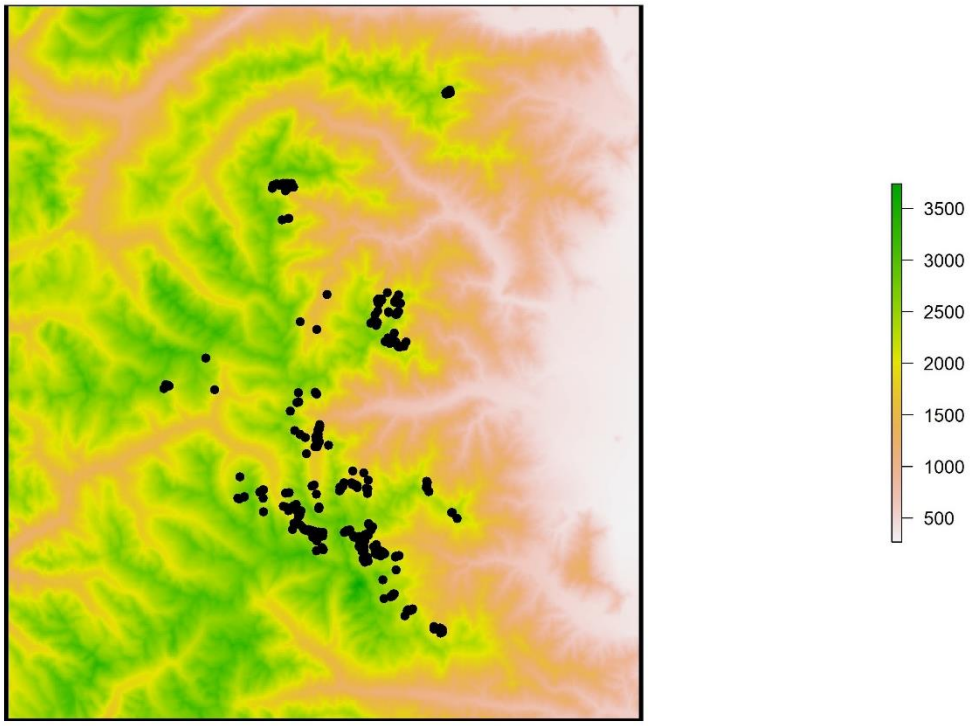

Figure S1.3 Physical map (Digital Terrain Model) reporting the position within the calibration area (black box) of the 360 occurrence points (black dots) of the Lanza's alpine salamander considered in the environmental and bioclimatic suitability modelling procedure. Elevation (in metres) is highlighted with different colours (see legend).

2. *Occurrence data*

The occurrence of the Lanza's alpine salamander is relatively well-documented throughout its range, especially in some easy-accessible and well-studied areas, where lots of observations are collected every year. In particular, some research and monitoring projects provided the bulk of the data, together with the research carried out independently by some herpetologists, the observations collected by park management authorities and citizen science (e.g. https://www.inaturalist.org).

Due to the large amount of available geo-referenced data (3382 records), often spatially autocorrelated, the final database considered in the modelling process is the result of a strict data selection procedure. First, a temporal selection was made, considering only the observations collected between the 01/01/2000 and the 31/12/2021. Secondly, only the geo-referenced data reporting a positional error <150 m were retained, in accordance with the spatial resolution of the predictor variables employed in the modelling procedure (~150 m). Lastly, in a further selection step, only one occurrence point was kept in each pixel of the predictor layers, in order to limit the spatial autocorrelation among observations, following the method described by Mammola et al. (2019). The resulting database includes 360 geo-referenced observations collected throughout all the known range of *S. lanzai* (Fig. S1.3).

3. Predictors

3.1 Current predictors

Three categories of predictors were considered to model the current environmental suitability for the Lanza's alpine Salamander within the calibration area, in accordance with the known ecological requirement of the species: (1) topographic, (2) bioclimatic and (3) environmental variables. Overall, 25 candidate parameters (4 topographic; 20 bioclimatic; and 1 environmental) were included as raster files in the first phase of the modelling procedure (Table 1, main text), all arranged to a spatial resolution of ~150 m (see Appendix S1.4 for upscaling and downscaling methods), as a trade-off between the known dispersal capacity of *S. lanzai* (Andreone et al., 1999; Ribéron & Miaud, 2000) and the available computational power.

The 30 m-Digital Terrain Model (DTM) provided by the Shuttle Radar Topography Mission (SRTM) (Farr et al., 2007) represents the baseline topographic predictor, from which the other parameters describing the physical features of the calibration area were calculated, namely exposition, slope, and topographic position index (TPI).

Nineteen bioclimatic variables were generated through the function *biovars()* in the *dismo* package (ver. 1.3-3; Hijmans et al., 2020) in *R* (ver. 4.2.2; R Core Team, 2022), starting from the monthly minimum temperature, maximum temperature and precipitation data (averaged on the 1970-2000 period) provided by WorldClim 2.1 (Fick & Hijmans, 2017) with a ~1 Km resolution (30 arcsec). These predictors were preferred to the raw temperature and precipitations parameters because they provide a useful summary of the biologically significant climatic conditions of a given area, including information on annual climatic conditions, as well as seasonal mean climate and intra-year seasonality. In addition, total monthly solar radiation data (average 1970-2000, ~1 Km resolution) were also gathered from WorldClim 2.1 (Fick & Hijmans, 2017), focusing in particular on the monthly values of June. This month was selected because it corresponds to the maximum solar radiation rates throughout the year in the study area, supposing that insolation represents a limiting factor for Lanza's alpine salamanders, often hidden underground in sunny days (Andreone et al., 1999).

Concerning environmental variables, most of the habitat features potentially important in shaping the distribution of *S. lanzai* are not easy to map on a wide geographical scale (e.g. vegetation composition, habitat type, availability of underground habitats, etc.). However, through remote sensing, several parameters are available to approximate the existing habitat conditions (at least on soil surface) even on large areas, as for instance vegetation indices. In particular, the Normalized Difference Vegetation Index (NDVI; Kriegler et al., 1969) is a remote-sensed indicator of photosynthetic activity ("greenness") of the biomes, basing on the principle that photosynthetic active vegetation absorbs most of the red light, while reflecting most of the near-infrared light. Many factors might affect NDVI values, such as plant photosynthetic activity, total plant cover, biomass, plant and soil moisture, and plant stress. Accordingly, NDVI is correlated with many ecosystem attributes (e.g. net primary productivity, canopy cover, bare ground cover, snow cover, etc.), making it a good proxy to describe habitat conditions (Pettorelli et al., 2005). Starting from the monthly NDVI values (averaged on the 2003-2020 period) provided by MODIS/Terra (MOD13A3, version 061. MODIS/Terra Vegetation Indices Monthly L3 Global 1 km SIN Grid; Didan, 2021) with a

spatial resolution of ~1 Km, the mean NDVI of July was gathered as environmental predictor in the modelling process. This month was selected because of its correspondence with the highest NDVI values throughout the year in alpine ecosystems, even at high elevations (Asam et al., 2018), thus revealing the peak of the photosynthetic activity in the study area during the Lanza's alpine salamander's activity period.

3.2 Predictor selection

Before to proceed with the *S. lanzai*'s environmental suitability modelling, a selection was made among the 25 candidate predictors described in the paragraph 3.1, basing in particular on their inter-correlation and on their contribution to the model outputs (the so-called "variable importance"). Since the use of strongly correlated variables may produce errors in model predictions, the possible occurrence of groups of inter-correlated parameters has been investigated, identifying the most representative predictor within each group, afterwards considered in the final modelling procedure. Firstly, according to the method proposed by Leroy et al. (2013) and with the recommendations provided by Barbet-Massin et al. (2012), 100 runs of 500 randomly-selected pseudo-absence points were generated throughout the model calibration area (Fig. S1.4), excluding a 150 m-buffer area around the Lanza's alpine salamander's occurrence points to avoid pseudo-replication (corresponding to the maximum positional error admitted for occurrence data and to the spatial resolution of predictor layers). In each run, pseudo-absence and occurrence data were merged in a single database, associating to each point the corresponding value of each one of the 25 candidate variables. Then, through the calculation of the Pearsons's correlation coefficient (r) and the generation of distance matrices among variables (where distance: $d = 1-r$), a final dendrogram was built, in order to graphically highlight the groups of inter-correlated variables, considering a threshold of $r = 0.8$ ($d = 0.2$) (Fig. S1.5). In this way, three groups of correlated predictors were identified (Fig. S1.5; Table S1.1): (1) a first one grouping temperature-related predictors, including elevation (DTM); while (2) the second and (3) the third groups encompass precipitations-related parameters.

In a second step, environmental suitability models were run using the 100% of the occurrence data, applying the same settings used in the final model configuration (see paragraph 5), but considering separately each group of inter-correlated predictors. Thanks to the variable importance estimation tool included in the *BIOMOD_Modeling()* function in the *biomod2* package (ver. 4.2.2; Thuiller et al., 2023) in *R* (ver. 4.2.2; R Core Team, 2022), the variable importance of each parameter within each group was calculated. The predictors with the highest variable importance values were promoted to the next modelling phase (Table S1.1), namely *Bio06*, *Bio12* and *Bio15*.

Once the inter-correlation issue was resolved, a final variable selection procedure was performed, by running again the models (100% occurrence data; same settings as final models) with the 6 non-correlated predictors (i.e. *TPI*, *Exp*, *Srad06*, *NDVI07*, *Slo* and *Bio09*) and the 3 parameters resulted from the inter-correlation analysis (i.e. *Bio06*, *Bio12* and *Bio15*). Through the variable importance tool of the *biomod2* package (Thuiller et al., 2023), the most relevant predictors in explaining the current distribution of the Lanza's alpine Salamander were identified (Table S1.2), and then considered in the environmental suitability model calibrated on the current scenario. The total solar radiation in June (*Srad06*)

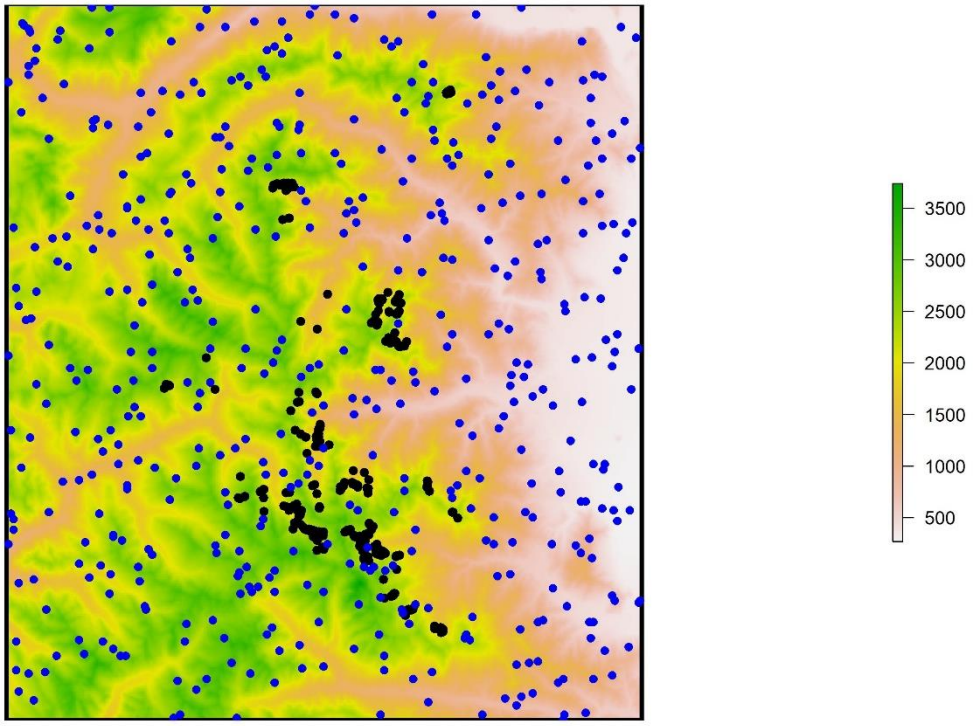

Figure S1.4 Physical map (Digital Terrain Model) reporting an example of 500 pseudo-absence points (blue dots) generated within the model calibration area (black box). The Lanza's alpine salamander's occurrence points are also reported in black. Elevation (in metres) is highlighted with different colours (see legend).

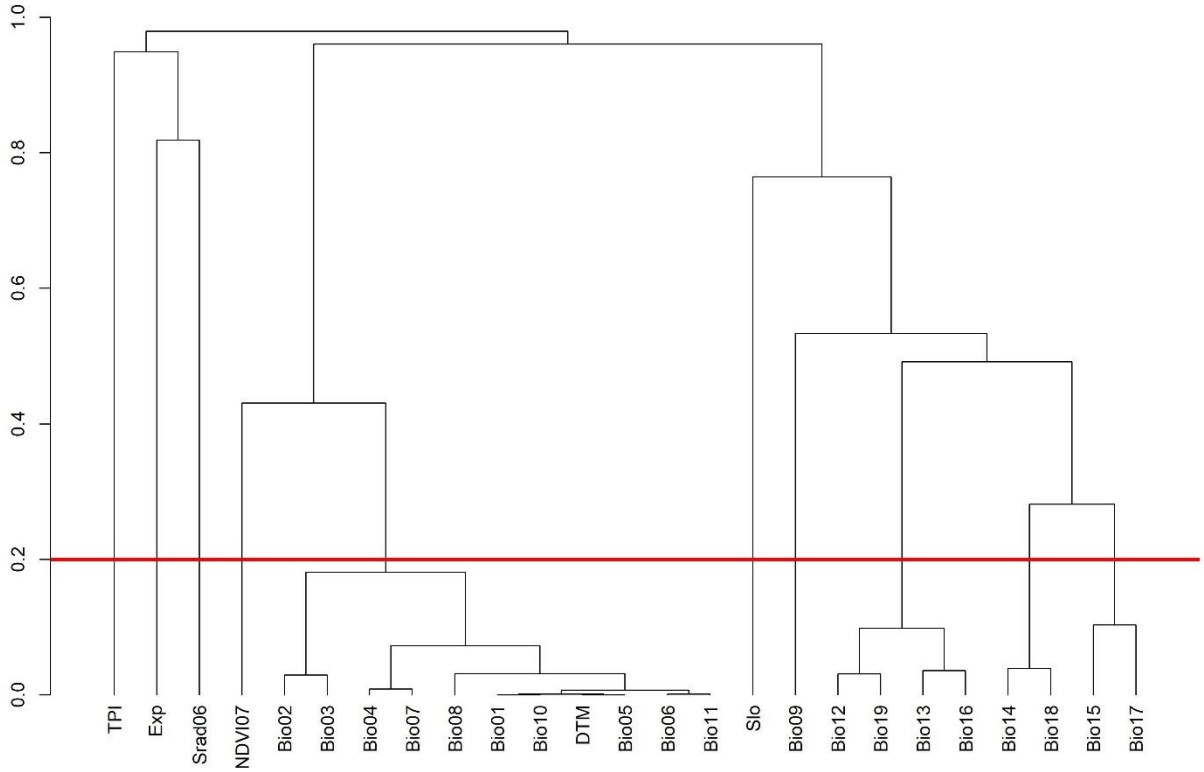

Figure S1.5 Dendrogram highlighting the inter-correlation among the 25 candidate predictors considered in the first phase of the environmental and bioclimatic suitability modelling process regarding *S. lanzai*, based on the distance parameter (d = 1-*r*), where *r* is the Pearson's correlation coefficient. The red line corresponds to the d = 0.2 (*r* = 0.8) threshold. Clusters below the red line encompass correlated parameters.

Table S1.1 Variable importance calculated within each group of inter-correlated predictors, as provided by the *biomod2* package. Code and description of each parameter are also reported. The highest variable importance values within each group are highlighted in bold, indicating the predictor promoted to the next modelling phase.

Group	Predictor	Description	Variable importance
Group 1	***Bio06***	**Min temperature of coldest month**	**0.587**
	DTM	Elevation	0.457
	Bio07	Temperature annual range	0.316
	Bio05	Max temperature of warmest month	0.260
	Bio01	Mean annual temperature	0.258
	Bio11	Mean temperature of coldest quarter	0.251
	Bio03	Isothermality	0.246
	Bio02	Mean diurnal range	0.221
	Bio08	Mean temperature of the wettest quarter	0.218
	Bio10	Mean temperature of warmest quarter	0.161
	Bio04	Temperature seasonality	0.122
Group 2	***Bio12***	**Total annual precipitation**	**0.659**
	Bio16	Precipitation of wettest quarter	0.466
	Bio19	Precipitation of coldest quarter	0.296
	Bio13	Precipitation of wettest month	0.224
Group 3	***Bio15***	**Precipitation seasonality**	**0.742**
	Bio18	Precipitation of warmest quarter	0.587
	Bio14	Precipitation of driest month	0.568
	Bio17	Precipitation of driest quarter	0.373

Table S1.2 Results of the final predictor selection (environmental suitability model), reported in terms of variable importance, as provided by the *biomod2* package. Code and description of each parameter are also reported. The variables selected for the final environmental suitability model calibration are highlighted in bold.

Predictor	Description	Variable importance
Srad06	**Total solar radiation June**	**0.342**
Bio06	**Min temperature of coldest month**	**0.274**
Bio12	**Total annual precipitation**	**0.228**
NDVI07	**NDVI July**	**0.210**
Bio09	**Mean temperature of driest quarter**	**0.176**
Bio15	Precipitation seasonality	0.089
TPI	Topographic Position Index	0.070
Exp	Exposition	0.020
Slo	Slope	0.020

Table S1.3 Results of the final predictor selection (bioclimatic suitability model), reported in terms of variable importance, as provided by the *biomod2* package. Code and description of each parameter are also reported. The variables selected for the final bioclimatic suitability model calibration are highlighted in bold.

Predictor	Description	Variable importance
Bio06	**Min temperature of coldest month**	**0.407**
Bio15	**Precipitation seasonality**	**0.362**
Bio12	**Total annual precipitation**	**0.326**
Bio09	**Mean temperature of driest quarter**	**0.260**
TPI	Topographic Position Index	0.100
Exp	Exposition	0.041
Slo	Slope	0.025

proved to be the most important predictor, followed by the minimum temperature of the coldest month (*Bio06*), total annual precipitations (*Bio12*), the NDVI values of July (*NDVI07*), and the mean temperature of the driest quarter of the year (*Bio09*). Instead, the precipitation seasonality (*Bio15*) and the remaining topographic parameters (*TPI*, *Exp* and *Slo*) showed the lowest variable importance values, being therefore excluded from the final environmental suitability model calibration.

Since simulations on the future distribution of *S. lanzai* require the availability of future projections of the environmental parameters considered in the current model predictions, a second variable selection process was carried out considering only topographic and bioclimatic variables. Indeed, future projections are available only for temperature and precipitation data, while topography can be assumed as a constant parameter, due to the negligible variations that might happen in the next century. Therefore, the final variable selection procedure described above has been repeated with the 4 non-correlated topographic and bioclimatic predictors (i.e. *TPI*, *Exp*, *Slo* and *Bio09*) and the 3 bioclimatic parameters resulted from the inter-correlation analysis (i.e. *Bio06*, *Bio12* and *Bio15*), identifying the most relevant topo-climatic predictors to be used to model the current and future bioclimatic suitability for *S. lanzai* (Table S1.3). The minimum temperature of the coldest month (*Bio06*) showed the highest variable importance value, followed by precipitation seasonality (*Bio15*), total annual precipitations (*Bio12*), and mean temperature of the driest quarter of the year (*Bio09*). On the other hand, the topographic parameters (i.e. *TPI*, *Exp* and *Slo*) proved to be less important, being therefore excluded from the final bioclimatic suitability model calibration.

3.3 Future predictors

As for current predictions, the four variables selected to model the future bioclimatic suitability for the Lanza's alpine salamander (*Bio06*, *Bio09*, *Bio12* and *Bio15*) were generated through the function *biovars()* in the *dismo* package (ver. 1.3-3; Hijmans et al., 2020) in *R* (ver. 4.2.2; R Core Team, 2022). In this case, the baseline data (i.e. monthly minimum temperature, maximum temperature and precipitations) were obtained from the CMIP6 downscaled future climate projections available in WorldClim 2.1 (~1 Km resolution, 30 arcsec; Fick & Hijmans, 2017), according to three different Global Circulation Models (GCMs) and two Shared Socio-economic Pathways (SSPs; i.e. CO_2 emission scenarios; Meinshausen et al., 2020) in two time periods.

Since GCMs often differ in initial conditions and mathematical models from which they are built, the use of different climate projections is highly recommended to reduce uncertainty in short- and long-term predictions of species distribution, especially if related to climate change (Buisson et al., 2010). However, some GCMs proved to be interdependent among themselves (Sanderson et al., 2015), thus requiring caution in their selection. Following the suggestions provided by Sanderson et al. (2015), the Australian Community Climate and Earth System Simulator's Earth System Model version 1.5 (ACCESS-ESM1-5), the Max Planck Institute Earth System Model at high resolution version 1.2 (MPI-ESM1-2-HR) and the sixth version of the Model for Interdisciplinary Research on Climate (MIROC6) were selected as independent GCMs to model the future distribution of *S. lanzai*. From each GCM, the SSP126 (low CO_2 emissions) and the SSP585 (high CO_2 emissions) climate projections were extracted for the calibration area, considering both a short-term (2041-2060) and a long-term (2081-2100) reference period. Accordingly, 12 different projections of the selected variables were considered to predict the future bioclimatic suitability for the Lanza's alpine salamander (i.e. 3 GCMs x 2 SSPs x 2 periods).

4. *Upscaling and downscaling methods*

Due to the limited dispersal capacity of the Lanza's alpine salamander (Andreone et al., 1999; Ribéron & Miaud, 2000) and to the complexity of the alpine habitats in which this amphibian occurs, predictors should have a relatively high spatial resolution in order to fit with the actual ecological features of the species. Given that pixel dimensions in the source raster files ranges from ~30 m to ~1 Km, an alignment to the lowest available resolution (i.e. ~1 Km) might be not appropriate, likely being too coarse to successfully meet the aims of our study. Therefore, following the example of Patsiou et al. (2014) and Mammola et al. (2019) concerning other alpine endemic plant and animal species, all predictors were upscaled or downscaled to a resolution of ~150 m, considered a suitable spatial scale according to the ecology of *S. lanzai*. Accordingly, before to calculate additional topographic variables, the SRTM's 30 m-Digital Terrain Model (DTM) has been upscaled, reducing of 5 times its resolution through the *aggregate()* function in the *raster* package (ver. 3.5-15; Hijmans, 2022) in *R* (ver. 4.2.2; R Core Team, 2022). This new DTM resolution was then used as reference to arrange all other predictor layers (i.e. those containing the bioclimatic and environmental variables).

A statistical downscaling procedure was applied to increase the spatial resolution of the original climatic (minimum temperature, maximum temperature, precipitation, and solar radiation) and environmental (NDVI) data, following Mammola et al. (2019). To downscale climatic data, two additional datasets were required: topographic descriptors from the upscaled SRTM's DTM (elevation, exposition, slope, and TPI) and climatic data (1981-2020) from 55 weather stations occurring within the calibration area to validate the results (Fig. S1.6). Monthly meteorological data were extracted from the ARPA Piemonte database (https://www.arpa.piemonte.it; downloaded at January 2022) and from the French meteorological and climatological office (https://donneespubliques.meteofrance.fr; downloaded at January 2022).

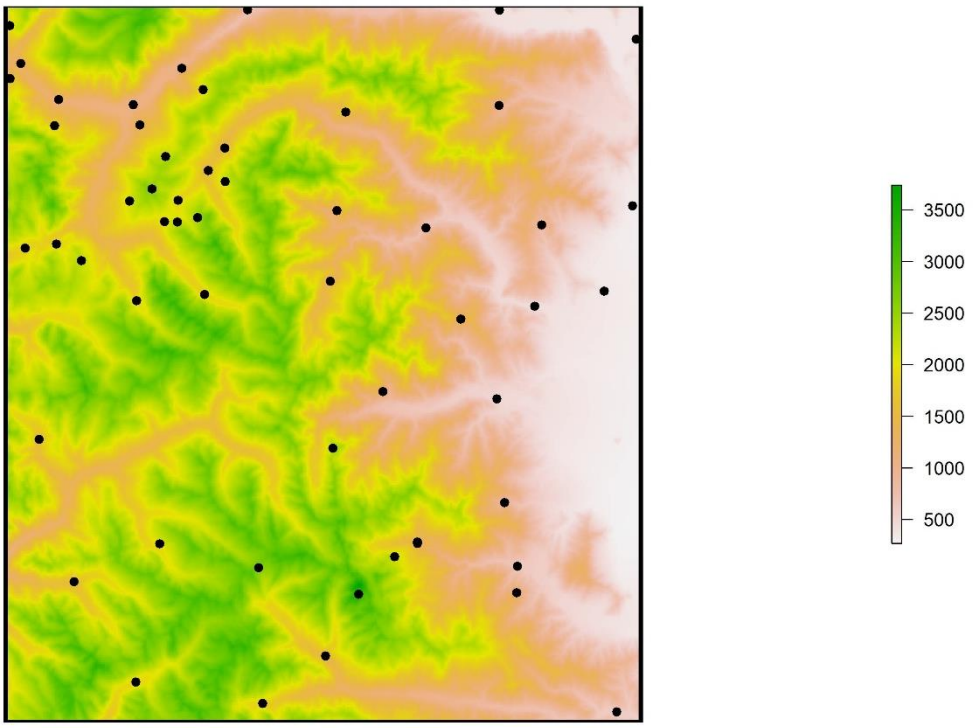

Figure S1.6 Physical map (Digital Terrain Model) reporting the position within the model calibration area (black box) of the 55 weather stations (black dots) used to validate the results of the statistical downscaling procedure concerning the climatic predictors (minimum temperature, maximum temperature, precipitations and solar radiation) involved in the environmental and bioclimatic modelling procedure. Elevation (in metres) is highlighted with different colours (see legend).

Table S1.4 Parameters used in the multiple linear regression procedure concerning minimum (Tmin) and maximum (Tmax) temperatures to assess downscaling model robustness. Values are referred to the best model identified for each month. R^2: determination coefficient; SE: standard error; RMSE: Root Mean Square Error; Delta: average error ± standard deviation between multiple linear regression results and the observed values in weather stations (N = 53). In addition, a comparison between kriging results and observed values in weather stations (Delta) is also reported, regarding monthly precipitations data (Prec; N = 40) and total solar radiation values (Srad; N = 15). Temperature values are in °C, precipitations are reported in mm, and solar radiation is in Kj/m^2.

Month	R^2		SE		RMSE		Delta			
	Tmin	Tmax	Tmin	Tmax	Tmin	Tmax	Tmin	Tmax	Prec	Srad
January	0.956	0.970	0.645	0.686	0.645	0.686	1.10±0.69	1.55±0.93	47.8±27.8	-
February	0.974	0.982	0.567	0.605	0.567	0.605	1.04±0.71	1.72±0.91	43.2±29.0	-
March	0.988	0.989	0.453	0.570	0.453	0.569	1.02±0.72	2.18±1.08	31.9±22.1	-
April	0.991	0.990	0.426	0.601	0.426	0.600	1.49±0.87	2.31±1.12	33.4±20.6	-
May	0.987	0.989	0.526	0.573	0.526	0.572	1.15±0.62	1.50±0.86	30.6±20.9	-
June	0.986	0.992	0.544	0.449	0.544	0.449	1.66±0.93	2.11±1.02	19.4±16.1	1220.4±793.4
July	0.980	0.991	0.598	0.450	0.598	0.449	1.18±0.77	1.29±0.98	14.5±10.5	-
August	0.975	0.990	0.605	0.430	0.605	0.429	1.11±0.85	1.14±0.85	16.4±10.7	-
September	0.978	0.991	0.555	0.409	0.555	0.409	1.09±0.83	0.91±0.66	19.9±14.4	-
October	0.978	0.990	0.490	0.409	0.490	0.409	0.93±0.68	0.81±0.48	26.9±20.5	-
November	0.976	0.983	0.459	0.502	0.459	0.502	0.98±0.74	1.09±0.60	55.8±29.7	-
December	0.960	0.974	0.578	0.593	0.577	0.593	1.08±0.71	1.08±0.74	41.8±30.3	-

Statistical downscaling of temperature data (minimum and maximum temperatures) was based on a multiple linear regression procedure, as described by Martin et al. (2013) and previously applied by Mammola et al. (2019). This method consists of refining climate data through the calculation of multiple linear regressions between the ~1 Km WorldClim 2.1 original data and the topographic descriptors at ~150 m resolution. Regressions were carried out iteratively, by deleting the worst descriptor at each iteration (backward elimination), considering each month of the year, without exploring links between months. Model robustness was measured via determination coefficient (R^2), standard error (SE), and Root Mean Square Error (RMSE). In addition, regressions were validated by comparing predicted values with the observed data extracted from weather stations (N = 53 with temperature data). Accordingly, at the end of the validation procedure, the models showing the lowest delta between predicted and observed values, the highest R^2, the lowest SE and the lowest RMSE were selected to finalize the downscaling process (Table S1.4).

The regression models selected after model validation show an R^2 between 0.956 and 0.991 for minimum temperatures and between 0.970 and 0.992 for maximum temperatures, while SE varies within the range 0.426-0.645 °C and 0.409-0.686 °C respectively. RMSE shows values between 0.426 and 0.645 °C for minimum temperatures and between 0.409 and 0.686 °C for maximum temperatures. The average errors between multiple linear regressions results and weather stations values are 1.15±0.76 °C and 1.47±0.85 °C for minimum temperatures and maximum temperatures respectively, showing variations among the modelled months. However, the statistical distribution of the predicted values is similar to the statistical distribution of the observed ones (i.e. gathered from weather stations), obviously depending from the distribution of the WorldClim 2.1 original data (Fig. S1.7).

Since multiple linear regressions usually produce unsatisfactory results in downscaling precipitation maps (Martin et al., 2013), a geostatistical interpolation method (kriging) was applied to increase the resolution of WorldClim 2.1 rainfall data, in order to allow at least a spatialization of precipitations in the calibration area (Mammola et al., 2019). The centroids of the original WorldClim 2.1 precipitation raster cells were used as input in the interpolation procedure, ran by means of the *krige()* function in the *gstat* package (ver. 2.0-7; Pebesma, 2004; Gräler et al., 2016) in *R* (ver. 4.2.2; R Core Team, 2022), after fitting a variogram model. The reliability of the downscaling procedure was then verified by comparing the downscaled data with those observed at each weather station (N = 40 with precipitations data).

The average error between kriging results and weather stations values is 31.8±13.2 mm, showing consistent variations among months (Table S1.4). In particular, cold months show higher Deltas between the predicted and observed precipitations (e.g. 55.8±29.7 mm in November) than the warmer ones (e.g. 14.5±10.5 mm in July), as also confirmed by the statistical distribution of the data (Fig. S1.8A). However, this error appears as an intrinsic feature of the source WorldClim 2.1 rainfall data in the calibration area, thus justifying the results obtained with the geostatistical interpolation.

The same method (kriging) was applied to downscale the WorldClim 2.1 solar radiation data of June, using 15 weather stations to verify results reliability. The average error between kriging results and weather stations values is 1220.4±793.4 Kj/m^2 (Table S1.4), with a statis-

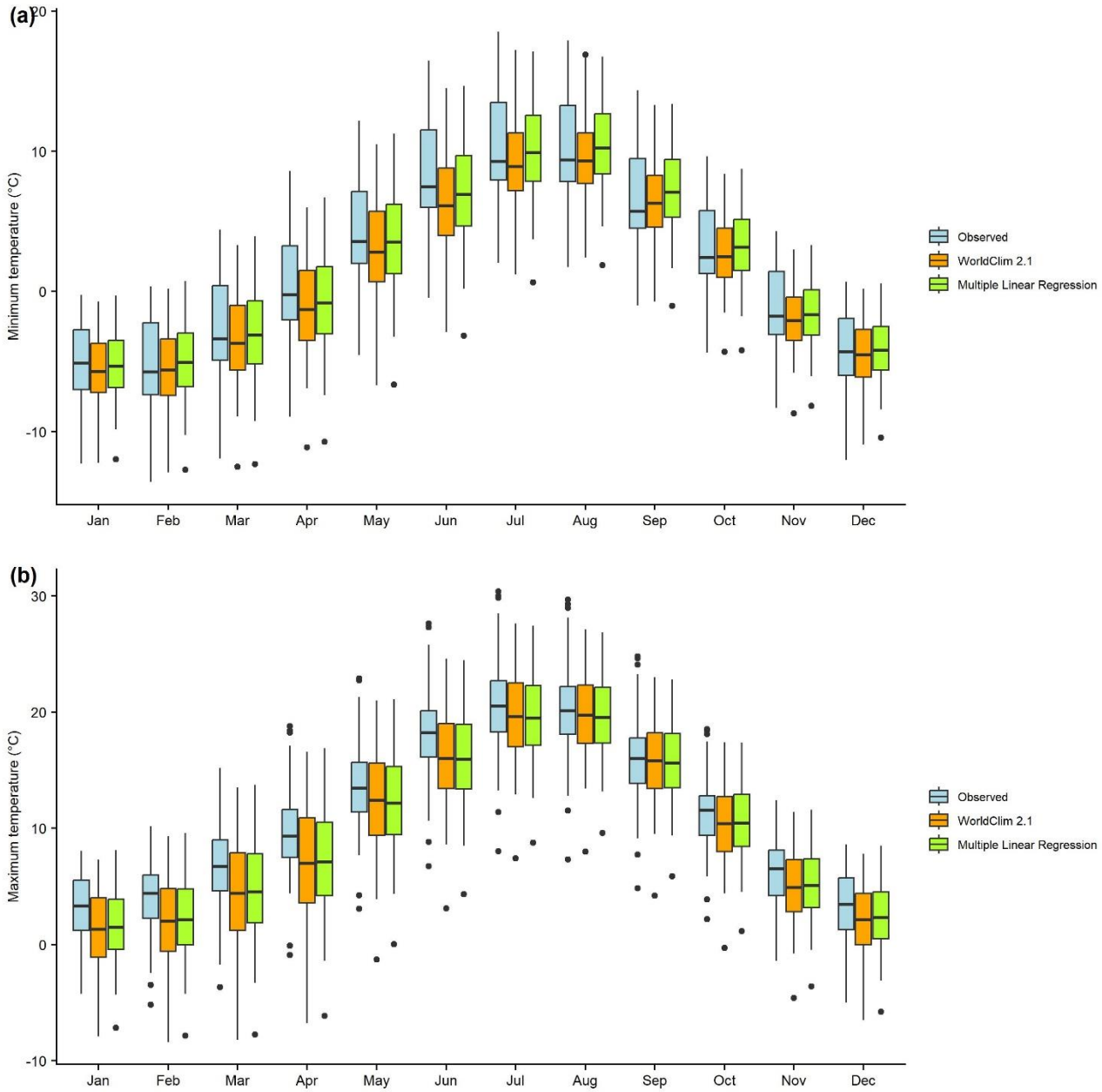

Figure S1.7 Statistical distribution of monthly minimum temperatures (**a**) and monthly maximum temperatures (**b**), showing the comparison between multiple linear regression results (green), WorldClim 2.1 original data (orange) and the observed values at weather stations (N = 53; light blue).

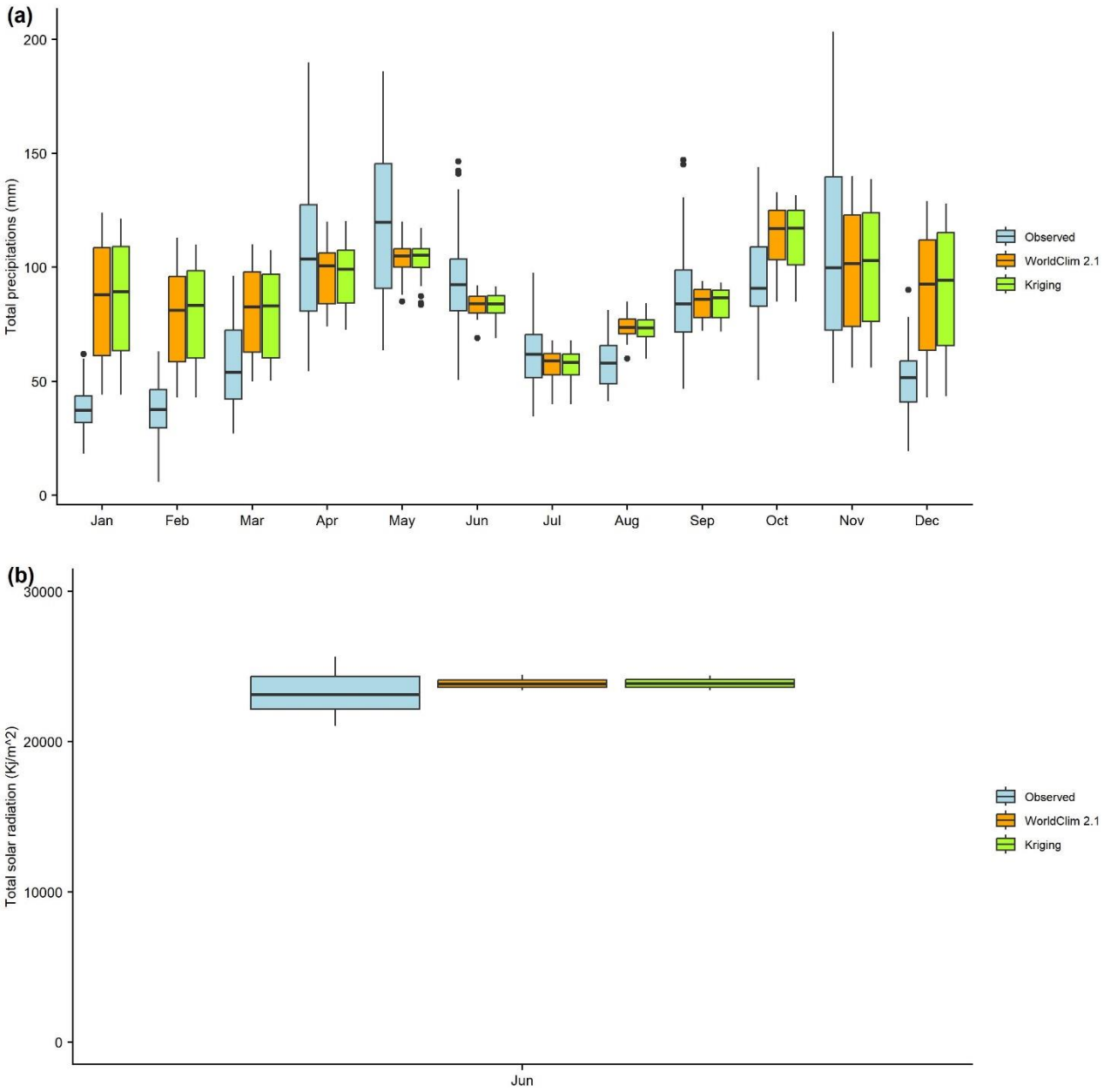

Figure S1.8 Statistical distribution of total monthly precipitations (**a**) and the total monthly solar radiation in June (**b**), showing the comparison between kriging results (green), WorldClim 2.1 original data (orange) and the observed values at weather stations (precipitations: N = 40; solar radiation: N = 15; light blue).

tical distribution of the predicted values similar to the distribution of the weather station data, also in accordance with WorldClim 2.1 predictions (Fig. S1.8B).
Finally, the kriging method was also applied to downscale the monthly NDVI layer of July. Unfortunately, in this case no validation datasets were available to confirm the reliability of the downscaling procedure.
The same procedure applied for current climate data was applied to increase the spatial resolution (from ~1 Km to ~150 m) of future projections of temperatures and precipitations. In particular, the same linear regressions used to downscale current temperature data (minimum and maximum temperatures; i.e. regressions that proved to minimize the difference between downscaled values and observed data in weather stations) were run again using future projections as dependent variable, while topographic descriptors were included as covariates, assuming a constant relationship between temperature and topography through time (i.e. same covariates used to downscale current and future data). Geostatistical interpolation (kriging) was also repeated with the same configuration used for current precipitation data, in order to increase the resolution of future rainfall predictions. In both cases, a validation dataset of observed data was obviously unavailable, thus we assume an error resulting from the downscaling procedure comparable with the one detected with current climate data.

5. *Modelling procedure*

Several algorithms are today available to run species distribution models (Peterson et al., 2011), each one with specific features. For this reason, the selection *a priori* of a single modelling technique (e.g. due to its convenience or ease of use) may provide unreliable results (Buisson et al., 2010; Qiao et al., 2015), since different algorithms might have a different predictive power. In order to overcome this issue (according to the procedure used by Leroy et al., 2013 and the recommendations provided by Buisson et al., 2010), an ensemble forecasting method (Araújo & New, 2007) has been implemented to predict the environmental and bioclimatic suitability for the Lanza's alpine salamander in the calibration area, involving 8 widely-used niche-based algorithms, all available in the *biomod2* package (ver. 4.2.2; Thuiller et al., 2023) in *R* (ver. 4.2.2; R Core Team, 2022): Generalized Boosting Model (GBM; Ridgeway, 1999), Classification Tree Analysis (CTA; Breiman et al., 1984), Flexible Discriminant Analysis (FDA; Hastie et al., 1994), Generalized Additive Models (GAM; Hastie & Tibshirani, 1990), Generalized Linear Models (GLM; McCullagh & Nelder, 1989), MaxEnt (MXT; Phillips et al., 2006), Multiple Adaptive Regression Splines (MARS; Friedman, 1991), and Random Forest (RF; Breiman, 2001).
Through the *BIOMOD_Modeling()* function (*biomod2* package; ver. 4.2.2; Thuiller et al., 2023), all the algorithms were run 10 times, each one corresponding to a randomly-selected series of 500 pseudo-absence points throughout the calibration area, excluding a 150 m-buffer zone around the occurrence points in order to avoid pseudo-replication. A spatial block cross-validation strategy (Muscarella et al., 2014) was applied to test models' predictive power (*BIOMOD_CrossValidation()* function in *biomod2*, ver. 4.2.2; Thuiller et al., 2023), then quantified by means of two evaluation metrics: the true skill statistic (TSS; Allouche et al., 2006) and the area under the relative operating characteristic curve (AUC; Fielding & Bell, 1997). Model robustness was evaluated 5 times per algorithm in each one of

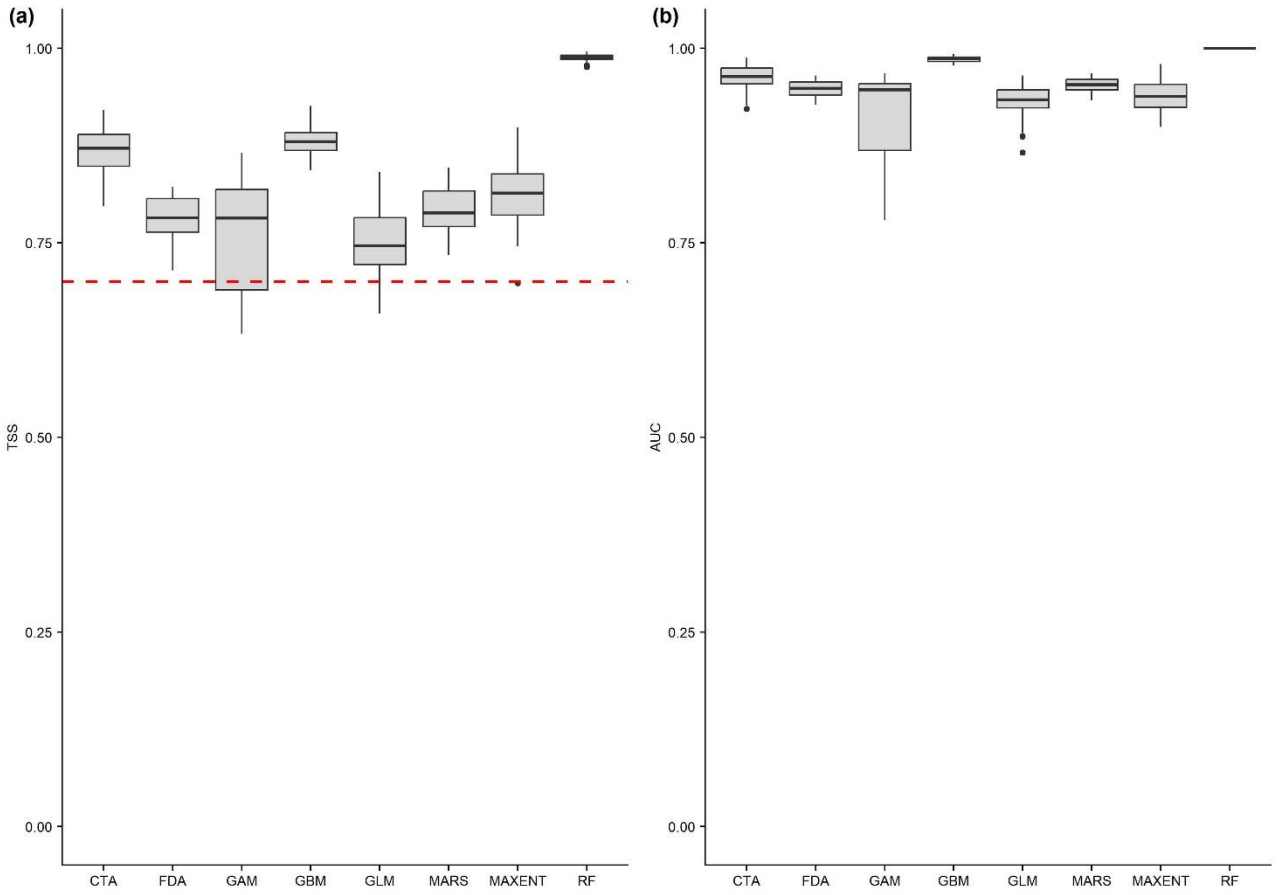

Figure S1.9 Statistical distribution of the evaluation metrics used to assess the environmental suitability model performances: (**a**) true skill statistic (TSS); (**b**) area under the relative operating characteristic curve (AUC). Each algorithm has been evaluated 5 times in each one of the 10 pseudo-absence runs (i.e. N = 50). In (**a**), the dashed red line corresponds to the TSS threshold value applied to select the models to be included in the ensemble forecast procedure (0.7).

the 10 performed runs, in order to obtain an average value of model performances, and the final models were calibrated on the 100% of the data. The response of *S. lanzai* in relation to the predictor variables involved in the modelling procedure was evaluated for each model, applying the evaluation strip method proposed by Elith et al. (2005), thanks to the *bm_PlotResponseCurves()* function in the *biomod2* package (ver. 4.2.2; Thuiller et al., 2023). In the environmental suitability model, most of the algorithms showed a good performance, with an average TSS of 0.832±0.079 and a mean AUC of 0.955±0.034 (Fig. S1.9). RF is the modelling technique that performed better, followed by GBM and CTA, while GAM and GLM showed the worst predictive power (Table 2, main text). Model runs with TSS evaluations below 0.7 (mainly GAMs) were discarded from the ensemble forecasting procedure, with consensus distributions resulting from the averaging of model predictions, proportionally weighted basing on their TSS evaluation. Final environmental suitability maps were then obtained by averaging ensemble forecasts from the 10 pseudo-absence runs. In addition, the original suitability maps were transformed into maps of suitable *vs* non-suitable areas (binary maps), by choosing the occurrence probability threshold that maximized the TSS value (Liu et al., 2005; Jiménez-Valverde & Lobo, 2007), as implemented in the *BIOMOD_EnsembleForecasting()* function in the *biomod2* package (ver. 4.2.2; Thuiller et al., 2023). The same procedure has then been applied to run the bioclimatic suitability model,

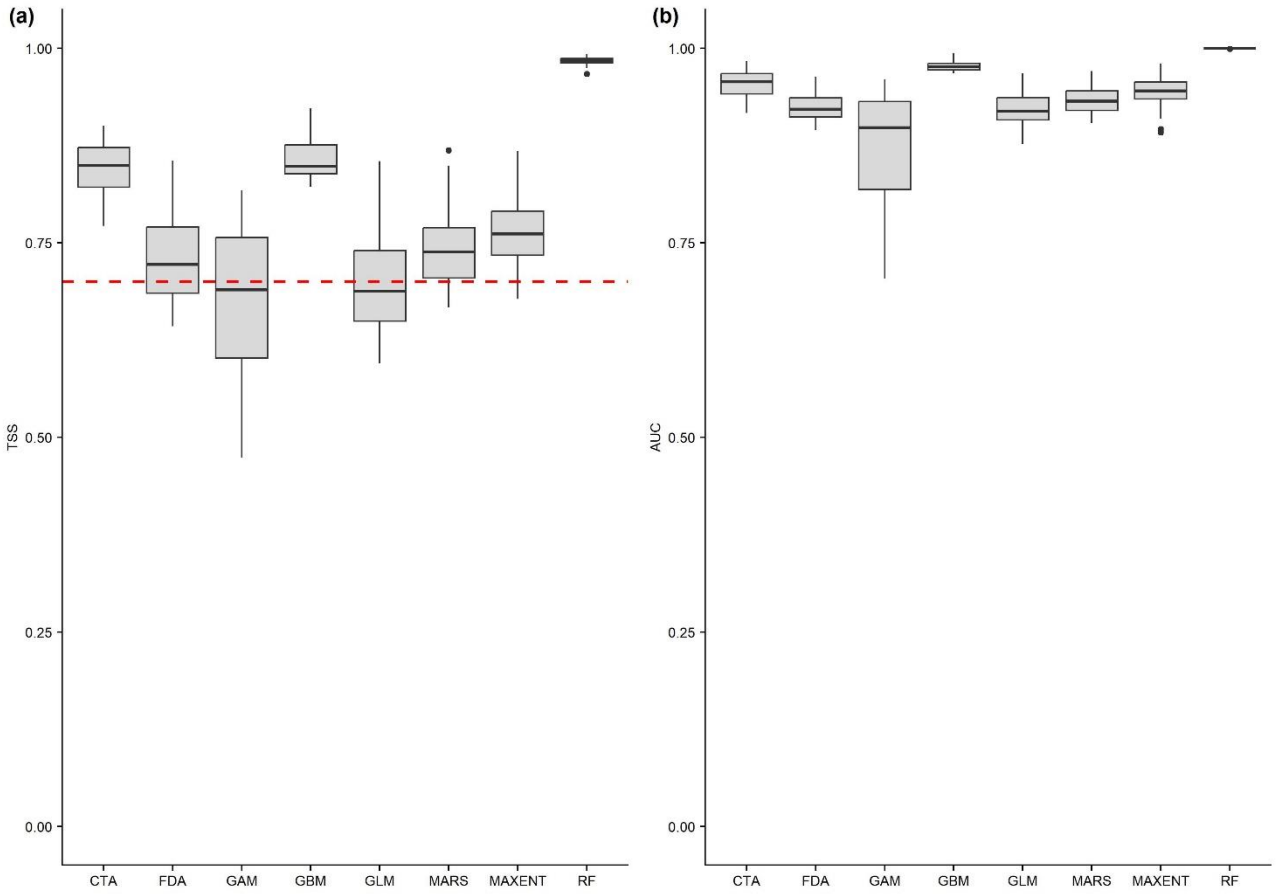

Figure S1.10 Statistical distribution of the evaluation metrics used to assess the bioclimatic suitability model performances: (**a**) true skill statistic (TSS); (**b**) area under the relative operating characteristic curve (AUC). Each algorithm has been evaluated 5 times in each one of the 10 pseudo-absence runs (i.e. N = 50). In (**a**), the dashed red line corresponds to the TSS threshold value applied to select the models to be included in the ensemble forecasting procedure (0.7).

obtaining similar results in terms of model performance, with RF as best performing algorithm, followed by GBM, CTA and MAXENT, while GAM and GLM showed the worst predictive power, with several runs below the TSS = 0.7 threshold (Fig. S1.10; Table 2, main text). In this case, TSS is in average 0.788±0.011, while the mean AUC is 0.942±0.044.

Lastly, future predictions were built starting from the current bioclimatic suitability model outputs, but considering the future projections of *Bio06*, *Bio09*, *Bio12* and *Bio15* as predictors. Firstly, 3 bioclimatic suitability maps and 3 binary maps were generated per time period and per SSP, according to the future predictions provided by the three GCMs considered. Then, final maps (N = 4, one per time period and per SSP) were obtained by averaging the results from the three GCMs. In binary maps, presence was attributed where the majority of GCMs (i.e. 2 out of 3) predicted presence, otherwise attributing absence.

6. References

Allouche, O., Tsoar, A. & Kadmon, R. (2006). Assessing the accuracy of species distribution models: prevalence, kappa and the true skill statistic (TSS). *Journal of Applied Ecology*, 43(6), 1223-1232. https://doi.org/10.1111/j.1365-2664.2006.01214.x

Andreone, F. (2006). *Salamandra lanzai*. In: *Atlas of Italian amphibians and reptiles*: 196-201. Sindaco, R., Doria, G., Razzetti, E. & Bernini, F. (eds). Societas Herpetologica Italica, Edizioni Polistampa, Firenze.

Andreone, F., Clima, V. & De Michelis, S. (1999). On the ecology of *Salamandra lanzai* (Nascetti, Andreone, Capula & Bullini, 1988). Number and movement of individuals, and influence of climate on activity in a population of the upper Po Valley (Caudata: Salamandridae). *Herpetozoa*, 12(1-2), 3-10.

Araújo, M.B. & New, M. (2007). Ensemble forecasting of species distributions. *Trends in Ecology & Evolution*, 22(1), 42-47. https://doi.org/10.1016/j.tree.2006.09.010

Asam, S., Callegari, M., Matiu, M., Fiore, G., De Gregorio, L., Jacob, A., Menzel, A., Zebisch, M. & Notarnicola, C. (2018). Relationship between spatiotemporal variations of climate, snow cover and plant phenology over the Alps - an earth observation-based analysis. *Remote Sensing*, 10(11), 1757. https://doi.org/10.3390/rs10111757

Barbet-Massin, M., Jiguet, F., Albert, C.H. & Thuiller, W. (2012). Selecting pseudo-absences for species distribution models: how, where and how many? *Methods in Ecology & Evolution,* 3(2), 327-338. https://doi.org/10.1111/j.2041-210X.2011.00172.x

Barve, N., Barve, V., Jiménez-Valverde, A., Lira-Noriega, A., Maher, S.P., Peterson, A.T., Soberón, S. & Villalobos, F. (2011). The crucial role of the accessible area in ecological niche modeling and species distribution modelling. *Ecological Modelling*, 222(11), 1810-1819. https://doi.org/10.1016/j.ecolmodel.2011.02.011

Breiman, L. (2001). Random forests. *Machine Learning*, 45, 5-32. https://doi.org/10.1023/A:1010933404324

Breiman, L., Friedman, J.H., Olshen, R.A. & Stone, C.J. (1984). Classification and regression trees. The Wadsworth Statistics Probability Series. Chapman & Hall, New York. https://doi.org/10.1201/9781315139470

Buisson, L., Thuiller, W., Casajus, N., Lek, S. & Grenouillet, G. (2010). Uncertainty in ensemble forecasting of species distribution. *Global Change Biology*, 16(4), 1145-1157. https://doi.org/10.1111/j.1365-2486.2009.02000.x

Didan, K. (2021). MODIS/Terra Vegetation Indices Monthly L3 Global 1km SIN Grid V061 [Data set]. NASA EOSDIS Land Processes DAAC. https://doi.org/10.5067/MODIS/MOD13A3.061. Downloaded at February 2022; https://search.earthdata.nasa.gov/search

Elith, J., Ferrier, S., Huettmann, F. & Leathwick, J. (2005). The evaluation strip: a new and robust method for plotting predicted responses from species distribution models. *Ecological Modelling*, 186(3), 280-289. https://doi.org/10.1016/j.ecolmodel.2004.12.007

Farr, T.G., Rosen, P.A., Caro, E., Crippen, R., Duren, R., Hensley, S., Kobrick, M., Paller, M., Rodriguez, E., Roth, L., Seal, D., Shaffer, S., Shimada, J., Umland, J., Werner, M., Oskin, M., Burbank, D. & Alsdorf, D. (2007). The Shuttle Radar Topography Mission. *Review in Geophysics.*, 45(2), RG2004. Downloaded at January 2022;

https://dwtkns.com/srtm30m/

Fick, S.E. & Hijmans, R.J. (2017). WorldClim 2: new 1-km spatial resolution climate surfaces for global land areas. *International Journal of Climatology*, 37(12), 4302-4315. Downloaded at January 2022; https://www.worldclim.org/data/worldclim21.html

Fielding, A.H. & Bell, J.F. (1997). A review of methods for the assessment of prediction errors in conservation presence/absence models. *Environmental Conservation*, 24(1), 38-49. https://doi.org/10.1017/S0376892997000088

Friedman, J.H. (1991). Multivariate adaptive regression splines. *The Annals of Statistics*, 19(1), 1-141. https://doi.org/10.1214/aos/1176347963

Gräler, B., Pebesma, E.J. & Heuvelink, G. (2016). Spatio-temporal interpolation using *gstat*. *The R Journal*, 8(1), 204-218.

Hastie, T. & Tibshirani, R. (1990). Generalized additive models. Chapman and Hall, London. https://doi.org/10.1201/9780203753781

Hastie, T., Tibshirani, R. & Buja, A. (1994). Flexible discriminant analysis by optimal scoring. *Journal of the American Statistical Association*, 89(428), 1255-1270. https://doi.org/10.1080/01621459.1994.10476866

Hijmans, R.J. (2022). *raster*: Geographic Data Analysis and Modeling. R package version 3.5-15. https://CRAN.R-project.org/package=raster

Hijmans, R.J., Phillips, S., Leathwick, J. & Elith, J. (2020). *dismo*: Species Distribution Modeling. R package version 1.3-3. https://CRAN.R-project.org/package=dismo

Jiménez-Valverde, A. & Lobo, J.M. (2007). Threshold criteria for conversion of probability of species presence to either–or presence–absence. *Acta Oecologica*, 31(3), 361-369. https://doi.org/10.1016/j.actao.2007.02.001

Kriegler, F.J., Malila, W.A., Nalepka, R.F. & Richardson, W. (1969). Preprocessing transformations and their effect on multispectral recognition. *Proceeding of the 6th International Symposium on Remote Sensing of Environment*, Ann Arbor, University of Michigan, 97-131.

Leroy, B., Paschetta, M., Canard, A., Bakkenes, M., Isaia, M. & Ysnel, F. (2013). First assessment of effects of global change on threatened spiders: potential impacts on *Dolomedes plantarius* (Clerck) and its conservation plans. *Biological Conservation*, 161, 155-163. https://doi.org/10.1016/j.biocon.2013.03.022

Liu, C., Berry, P.M., Dawson, T.P. & Pearson, R.G. (2005). Selecting thresholds of occurrence in the prediction of species distributions. *Ecography*, 28(3), 385-393. https://doi.org/10.1111/j.0906-7590.2005.03957.x

Mammola, S., Milano, F., Vignal, M., Andrieu, J. & Isaia, M. (2019). Associations between habitat quality, body size and reproductive fitness in the alpine endemic spider *Vesubia jugorum*. *Global Ecology and Biogeography*, 28(9), 1325-1335. https://doi.org/10.1111/geb.12935

Martin, N., Carrega, P. & Adnes, C. (2013). Downscaling a fine résolution spatiale des températures actuelles et futures par modélisation statistique des sorties ALADIN-Climat sur les Alpes-Maritimes (France). *Climatologie*, 10, 51-72. https://doi.org/10.4267/climatologie.109

McCullagh, P. & Nelder, J.A. (1989). Generalized linear models. Second Edition. Chapman and Hall, London. https://doi.org/10.1201/9780203753736

Meinshausen, M., Nicholls, Z.R.J., Lewis, J., Gidden, M.J., Vogel, E., Freund, M., Beyerle, U., Gessner, C., Nauels, A., Bauer, N., Canadell, J.C., Daniel, J.S., John, A., Krummel, P.B., Luderer, G., Meinshausen, N., Montzka, S.A., Rayner, P.J., Reimann, S., Smith, S.J., van den Berg, M., Velders, G.J.M., Vollmer, M.K. & Wang, R.H. (2020). The shared socio-economic pathway (SSP) greenhouse gas concentrations and their extensions to 2500. *Geoscientific Model Development*, 13(8), 3571-3605. https://doi.org/10.5194/gmd-13-3571-2020

Muscarella, R., Galante, P.J., Soley-Guardia, M., Boria, R.A., Kass, J.M., Uriarte, M. & Anderson, R.P. (2014). ENMeval: an R package for conducting spatially independent evaluations and estimating optimal model complexity for Maxent ecological niche models. *Methods in Ecology & Evolution*, 5(11), 1198-1205. https://doi.org/10.1111/2041-210X.12261

Patsiou, T.S., Conti, E., Zimmermann, N.E., Theodoridis, S. & Randin, C.F. (2014). Topo-climatic microrefugia explain the persistence of a rare endemic plant in the Alps during the last 21 millennia. *Global Change Biology*, 20(7), 2286-2300. https://doi.org/10.1111/gcb.12515

Pebesma, E.J. (2004). Multivariable geostatistics in S: the *gstat* package. *Computers & Geosciences*, 30, 683-691. https://github.com/r-spatial/gstat/

Peterson, A.T., Soberón, J., Pearson, R.G., Anderson, R.P., Martínez-Meyer, E., Nakamura, M. & Araújo, M.B. (2011). Ecological niches and geographic distributions. Princeton University Press. https://doi.org/10.23943/princeton/9780691136868.001.0001

Pettorelli, N., Vik, J.O., Mysterud, A., Gaillard, J.M., Tucker, C.J. & Stenseth, N.C. (2005). Using the satellite-derived NDVI to assess ecological responses to environmental change. *Trends in Ecology & Evolution*, 20(9), 503-510. https://doi.org/10.1016/j.tree.2005.05.011

Phillips, S.J., Anderson, R.P. & Schapire, R.E. (2006). Maximum entropy modeling of species geographic distributions. *Ecological Modelling*, 190(3-4), 231-259. https://doi.org/10.1016/j.ecolmodel.2005.03.026

Qiao, H., Soberón, J. & Peterson, A.T. (2015). No silver bullets in correlative ecological niche modelling: insights from testing among many potential algorithms for niche estimation. *Methods in Ecology & Evolution*, 6(10), 1126-1136. https://doi.org/10.1111/2041-210X.12397

R Core Team, 2022. *R*: A language and environment for statistical computing. *R* Foundation for Statistical Computing, Vienna, Austria. URL https://www.R-project.org/.

Ribéron, A. & Miaud, C. (2000). Home range and shelter use in *Salamandra lanzai* (Caudata, Salamandridae). *Amphibia-Reptilia*, 21(2), 255-260. https://doi.org/10.1163/156853800507390

Ridgeway, G. (1999). The state of boosting. *Computing Science and Statistics*, 31: 172-181. http://www.planchet.net/EXT/ISFA/1226.nsf/0/a29acbd26d902d6fc125822a0031c09b/$FILE/boosting.pdf

Sanderson, B.M., Knutti, R. & Caldwell, P. (2015). A representative democracy to reduce interdependency in a multimodel ensemble. *Journal of Climate*, 28(13), 5171-5194. https://doi.org/10.1175/JCLI-D-14-00362.1

Soberón, J. & Peterson, A.T. (2005). Interpretation of models of fundamental ecological niches and species' distributional areas. *Biodiversity Informatics*, 2, 1-10. https://doi.org/10.17161/bi.v2i0.4

Thuiller, W., Georges, D., Gueguen, M., Engler, R., Breiner, F., Lafourcade, B. & Patin, R. (2023). *biomod2*: ensemble platform for species distribution modeling. R package version 4.4.4. https://CRAN.R-project.org/package=biomod2

APPENDIX S2 – Supplementary figures

Figure S2.1 – Response curves, environmental suitability model

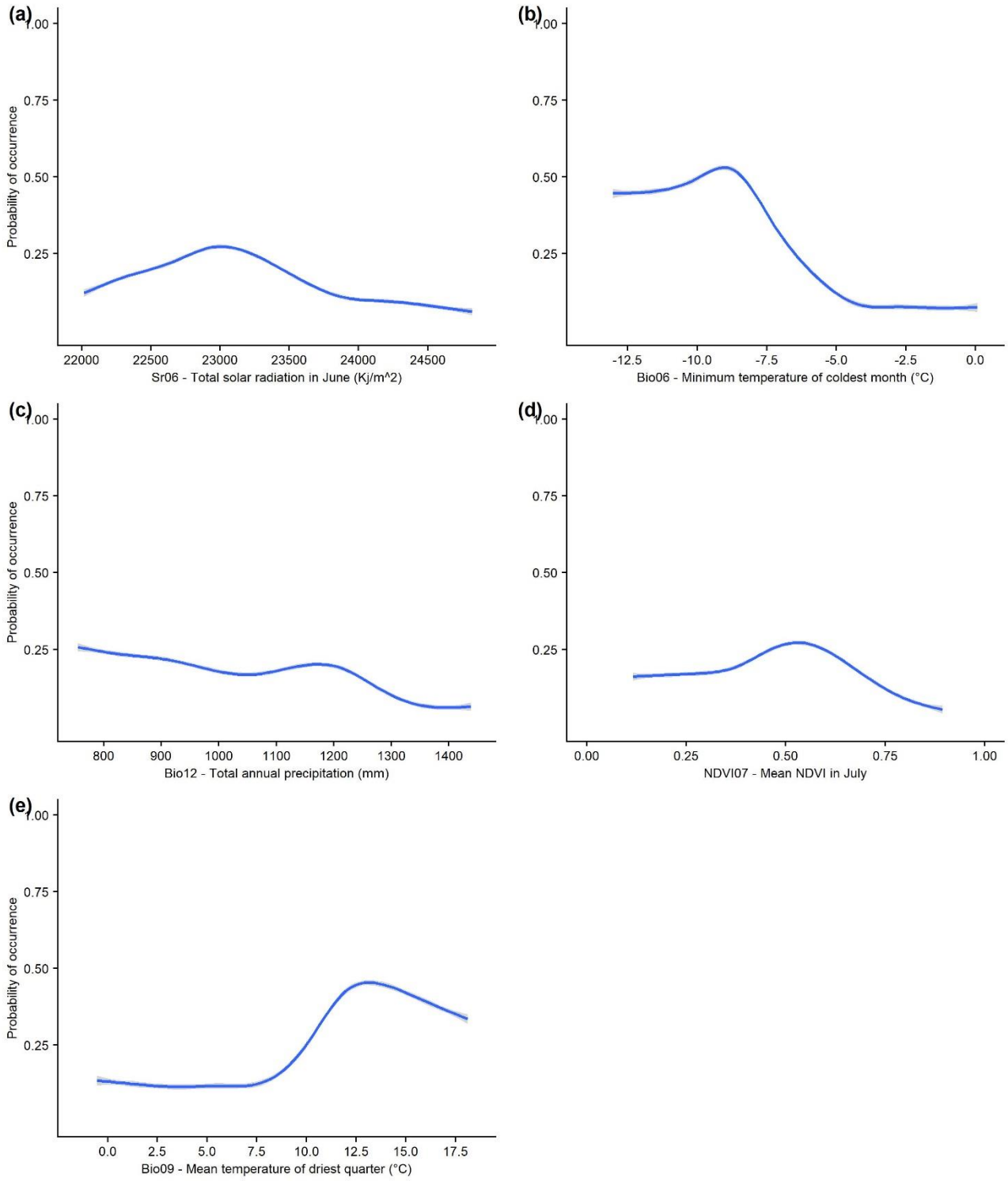

Figure S2.1. Probability of occurrence of *S. lanzai* in relation to the predictor variables involved in the environmental suitability modelling procedure. The blue line is the fitted GAM function based on all the response curves from the 10 pseudo-absence runs and the 8 algorithms considered. The grey area represents the 95% confidence interval. The range of values along the x axis is the range of existing values in the whole calibration area.

Figure S2.2 – Response curves, bioclimatic suitability model

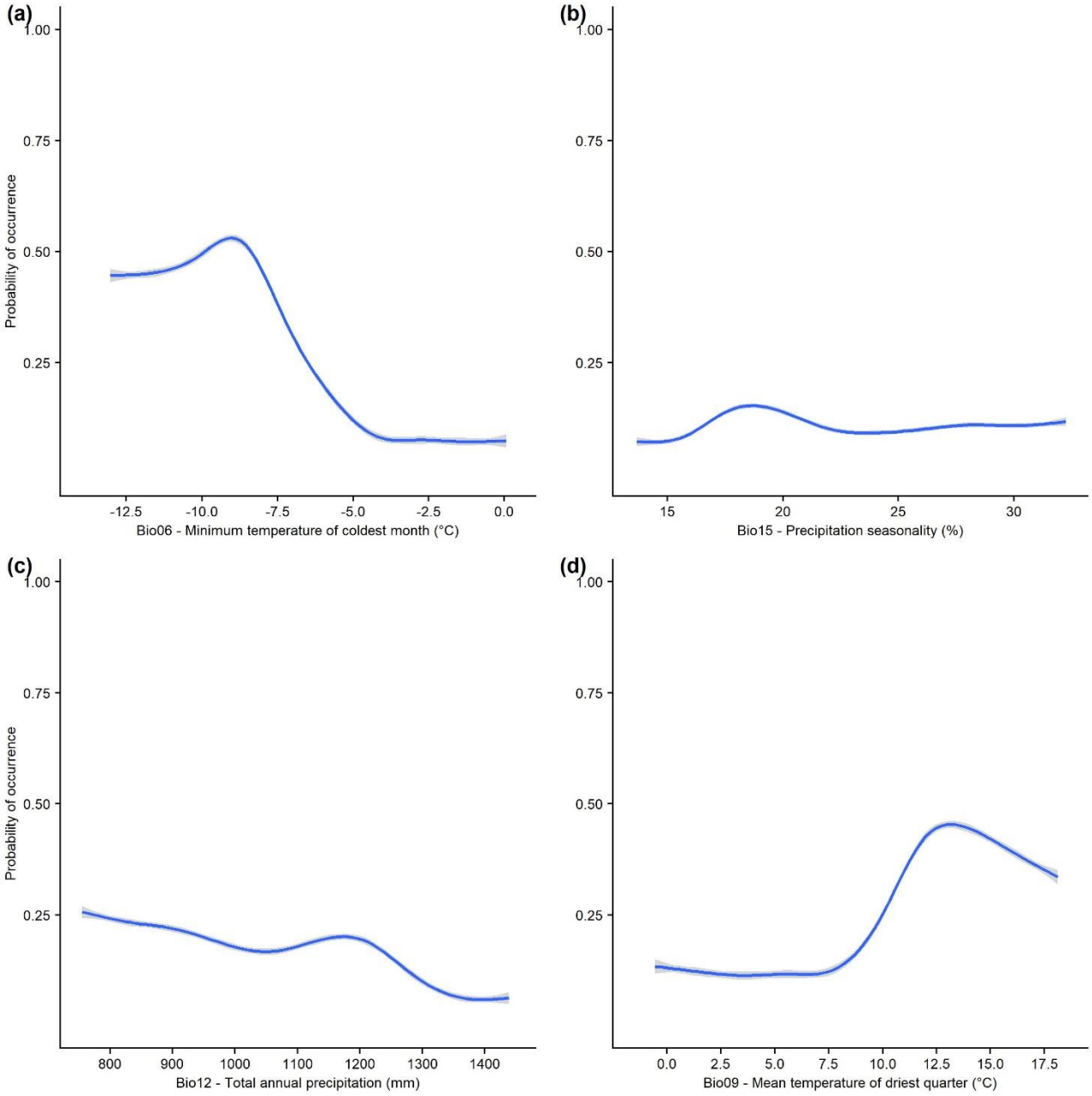

Figure S2.2. Probability of occurrence of *S. lanzai* in relation to the predictor variables involved in the bioclimatic suitability modelling procedure. The blue line is the fitted GAM function based on all the response curves from the 10 pseudo-absence runs and the 8 algorithms considered. The grey area represents the 95% confidence interval. The range of values along the x axis is the range of existing values in the whole calibration area.

Figure S2.3 – Temporal trend of bioclimatic predictors

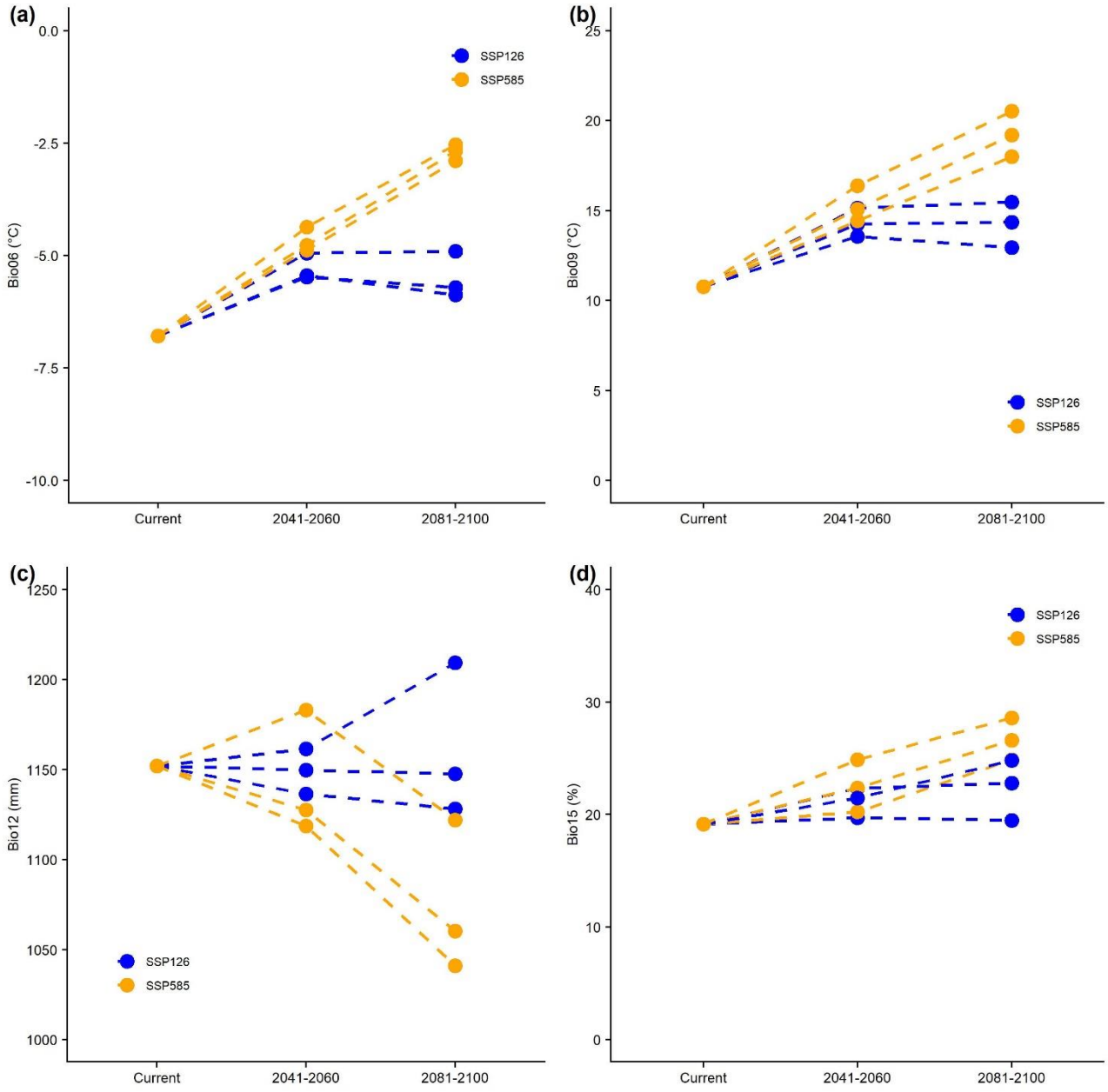

Figure S2.3. Temporal trend of the four bioclimatic predictors involved in the calibration of the bioclimatic suitability model, according to the time periods and the SSPs considered in the modelling procedure. **a**: *Bio06* - Minimum temperature of the coldest month; **b**: *Bio09* - Mean temperature of the driest quarter; **c**: *Bio12* – Total annual precipitation; **d**: *Bio15* – Precipitation seasonality.

APPENDIX S3 – Supplementary information

1. *Model uncertainties*

As often happens in species distribution model (SDM) forecasts (Beale & Lennon, 2012), the results presented in this paper are not free from uncertainties, depending on models' structure, the algorithms used, the amount and quality of occurrence data, and mismatches between modelling and data scales (Thuiller, 2004; Wiens et al., 2009). In general, the biological realism of SDMs is enhanced through an adequate understanding of the underlying assumptions, evaluating their potential effects, and, when possible, by incorporating additional details into the models, as for instance demography, dispersal, landscape effects, biotic interactions, and any mechanistic factor involved in species' response to biophysical conditions (Kearney & Porter, 2009; Wiens et al., 2009; Franklin 2010).

In the case of the Lanza's alpine salamander, a first conceptual source of uncertainty depends from the correlative approach used in the modelling procedure, simply linking environmental and bioclimatic data to distribution records, which leads to model only the realized (i.e. ecological) niche of the species. This strategy excludes all the mechanistic links between *S. lanzai*'s functional traits and environmental conditions, preventing the projections through space and time of the fundamental (i.e. physiological) niche, often involved in constraining species distributions (Kearney & Porter, 2009).

Secondly, although ensemble models allow to reduce the misleading effect of the different predictive power of different algorithms (Araújo & New, 2007), with performance statistics ensuring a valuable assessment of model robustness, possible errors in model outcomes may result from the lack of correspondence between broad-scale predictors and the actual environmental and bioclimatic conditions occurring in the Lanza's alpine salamander's range.

For instance, the temporal mismatch between the observations of *S. lanzai* (2000-2021) and the WordlClim 2.1 raw climate data (averaged on the 1970-2000 period; Fick & Hijmans, 2017) provides a first possible source of error in the temperature, precipitation, and solar radiation values truly experienced by this species in the calibration area, thus potentially conditioning the reliability of current and future projections based on bioclimatic parameters. By comparing the WordlClim 2.1 downscaled data with the observed records in 55 weather stations scattered within the calibration area (1981-2020 period), this error has been quantified in average as 1.15±0.76 °C for minimum temperatures, 1.47±0.85 °C for maximum temperatures, 31.8±13.2 mm for precipitations, and 1220.4±793.4 Kj/m^2 for solar radiation, showing variations among months (see Appendix S1.4). However, the observed temperature and solar radiation data follow the same statistical distribution of WorldClim 2.1 predictions throughout the year, thus limiting the uncertainty to the actual temperature and irradiation values preferred by *S. lanzai*, rather than its response to variations in space and time. On the other hand, the clear dissimilarities between observed and predicted precipitations data, with WorldClim 2.1 significantly overestimating rainfall (or snowfall) values in the coldest month of the year, may depend on the systematic error that affects rain gauges data, likely successfully corrected by Fick & Hijmans (2017). Indeed, comparative studies carried out in the Alps show that in winter rain gauges may underestimate the snow

water equivalent (SWE) in a range between 15% and 66% (Grossi et al., 2017), thus suggesting the actual reliability of the precipitation-related predictors involved in the modelling procedure.

As far the ensemble model outputs are concerned, the observed local mismatch between model predictions and species occurrence may depend from several factors, including data collection issues (leading to false absences) and shortcomings in models' predictive capacity (high suitability predicted where the species is actually absent). First of all, a detectability issue has to be considered when searching the Lanza's alpine salamander in the field, since the encounter probability of surface-dwelling individuals strongly depends on population density. Indeed, population density may vary considerably throughout the range of this species, ranging from 98.6 ind/ha (Seglie, 2019, unpublished report) up to 733.0 ind/ha (Eusebio Bergò, 2001, unpublished report), consequently increasing the risk of false negative results where low-density and localized populations occur. Therefore, to ascertain the true absence of *S. lanzai* is not an easy task, even when exploring environmentally and climatically suitable areas, also due to its predominant subterranean habits, thus preventing an unequivocal confutation of model predictions.

Conversely, wrong predictions by ensemble models cannot be locally excluded, especially whether biogeographical and environmental factors actually involved in shaping *S. lanzai*'s distribution have not been accounted in the modelling procedure. For instance, models may predict high suitability in mountain sectors that remained unreachable for Lanza's alpine salamanders throughout their biogeographical history, owing to the occurrence of unpredictable dispersal barriers within the calibration area. In addition, some key environmental factors, such as the local availability of suitable subterranean habitats, as well as microclimatic conditions, are not considered among predictors (e.g. no cartography available on the whole calibration area), possibly compromising models' predictive capacity in some areas.

The identification of a study area (as a subset of the models' calibration area), based on known occurrence data, targeted field surveys, and expert opinion, can partially reduce the risk of an overestimation in model projections, at least excluding out-of-reach suitable areas from spatial analyses and future predictions. However, detectability issues and fine-scale habitat features continue to represent a source of uncertainty, therefore suggesting caution when analysing in detail *S. lanzai*'s environmental and bioclimatic suitability maps, especially when management and conservation projects or land use changes are planned within the study area. In this case, the implementation of specific monitoring programs is always highly recommended, as additional information source to model outputs for decision-makers and land-managers.

2. *References*

Araújo, M.B. & New, M. (2007). Ensemble forecasting of species distributions. *Trends in Ecology & Evolution*, 22(1), 42-47. https://doi.org/10.1016/j.tree.2006.09.010

Beale, C.M. & Lennon, J.J. (2012). Incorporating uncertainty in predictive species distribution modelling. *Philosophical Transactions of the Royal Society B: Biological Sciences*, 367(1586), 247-258. https://doi.org/10.1098/rstb.2011.0178

Fick, S.E. & Hijmans, R.J. (2017). WorldClim 2: new 1-km spatial resolution climate surfaces for global land areas. *International Journal of Climatology*, 37(12), 4302-4315. Downloaded at January 2022; https://www.worldclim.org/data/worldclim21.html

Franklin, J. (2010). Moving beyond static species distribution models in support of conservation biogeography. *Diversity & Distributions*, 16(3), 321-330. https://doi.org/10.1111/j.1472-4642.2010.00641.x

Grossi, G., Lendvai, A., Peretti, G. & Ranzi, R. (2017). Snow precipitation measured by gauges: systematic error estimation and data series correction in the central Italian Alps. *Water*, 9(7), 461. https://doi.org/10.3390/w9070461

Kearney, M. & Porter, W. (2009). Mechanistic niche modelling: combining physiological and spatial data to predict species' ranges. *Ecology Letters*, 12(4), 334-350. https://doi.org/10.1111/j.1461-0248.2008.01277.x

Thuiller, W. (2004). Patterns and uncertainties of species' range shifts under climate change. *Global Change Biology*, 10(12), 2020-2027. https://doi.org/10.1111/j.1365-2486.2004.00859.x

Wiens, J.A., Stralberg, D., Jongsomjit, D., Howell, C.A. & Snyder, M.A. (2009). Niches, models, and climate change: assessing the assumptions and uncertainties. *Proceeding of the National Academy of Sciences*, 106(supplement_2), 19729-19736. https://doi.org/10.1073/pnas.0901639106